Received: 11 October 2017 | Accepted: 18 January 2018

DOI: 10.1002/jbio.201700299

Journal of BIOPHOTONICS

REVIEW ARTICLE

Biofluid spectroscopic disease diagnostics: A review on the processes and spectral impact of drying

James M. Cameron[1] | Holly J. Butler[1] | David S. Palmer[2] | Matthew J. Baker[1]*

[1]WestCHEM, Department of Pure and Applied Chemistry, Technology and Innovation Centre, University of Strathclyde, Glasgow, UK

[2]WestCHEM, Department of Pure and Applied Chemistry, University of Strathclyde, Glasgow, UK

*Correspondence
Dr Matthew J. Baker, WestCHEM, Department of Pure and Applied Chemistry, Technology and Innovation Centre, University of Strathclyde, 99 George Street, Glasgow G1 1RD, UK.
Email: matthew.baker@strath.ac.uk

Funding information
EPSRC, Grant/Award number: EP/L505080/1

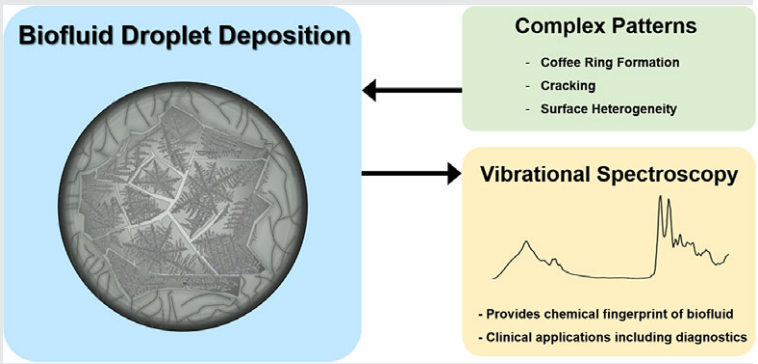

The complex patterns observed from evaporated liquid drops have been examined extensively over the last 20 years. Complete understanding of drop deposition is vital in many medical processes, and one which is essential to the translation of biofluid spectroscopic disease diagnostics. The promising use of spectroscopy in disease diagnosis has been hindered by the complicated patterns left by dried biological fluids which may inhibit the clinical translation of this technology. Coffee-ring formation, cracking and gelation patterns have all been observed in biofluid drops, and with surface homogeneity being a key element to many spectroscopic techniques, experimental issues have been found to arise. A better understanding of the fundamental processes involved in a drying droplet could allow efficient progression in this research field, and ultimately benefit the population with the development of a reliable cancer diagnostic.

KEYWORDS

biofluids, coffee ring, cracking, gelation, infrared, serum, spectroscopy, Vroman

1 | INTRODUCTION

Pattern formation in an evaporating liquid droplet is a complex process which has attracted a vast amount of research over the last few decades. The phenomenon is dependent on many complex physical mechanisms; such as fluid dynamics, phase transitions, heat transfer and contact line depinning [1–3], as well as the physical and chemical properties of the evaporating solution and solid surface [4, 5]. The complicated behaviour is of interest to many industrial and medical processes, as it plays an important role in various applications, such as inkjet printing, liquid coating, drug screening, bioassays and DNA printing [6–9]. More recently, the comprehension of this concept has become more desirable in the field of biomedical vibrational spectroscopy, with the emerging use of spectroscopic techniques in disease diagnostics [10, 11]. Despite the interest in this line of research, the concept is still not completely understood. The unusual patterns observed from dried drops of biological fluids can cause experimental issues [12], often preventing many proof-of-concept studies from progressing.

2 | FUNDAMENTALS OF DROPLET EVAPORATION

When a liquid droplet is introduced to a flat, horizontal surface, a "contact line" is formed, which is the intersection of the liquid-solid and liquid-vapour interfaces. The point at which solid, liquid and vapour coexist is known as the triple-phase line, as shown in Figure 1 [13]. The angle between the contact line and the solid surface, known as the contact angle (θ_Y), can be estimated theoretically by Eq. (1), first described by Thomas Young [14] in 1805;

$$\gamma_{lv}\cos\theta_Y = \gamma_{sv} - \gamma_{sl} \quad (1)$$

The concept of "wettability" can be described as the tendency of a fluid to adhere to a particular solid surface [15]. In general, the wettability of a surface is better where there is a contact angle of $\theta < 90°$, as wetting is favoured and the liquid spreads over a larger area of the surface—these can be described as hydrophilic. Conversely, hydrophobic surfaces have contact angles of $\theta > 90°$, and hence have poor wettability, where the fluid minimises contact with the surface causing a more rigid droplet [16]. The shape of the droplet, and therefore the contact angle, is mainly determined by the surface tension – which is caused by the unbalanced forces of the liquid molecules that are present at the surface of the drop [13]. Recently there has been interest in "superhydrophobic" surfaces, which are associated with extremely high contact angles—$\theta > 150°$. These surfaces are found to be very difficult to wet, where a droplet sits on top of the surface, retaining an almost spherical shape [17].

The well-known Young's equation gives a theoretical value in ideal conditions (ie, a smooth and homogeneous surface); however, in reality, the contact angle usually is not exactly equal to θ_Y. This is because on a "non-ideal" surface, the contact angle is dynamic, and so cannot be described by one unique value. The liquid drop can both expand, forming advancing contact angles, θ_a, and contract, causing receding contact angles, θ_r [13]. The difference between the angles is defined as contact angle hysteresis (CAH), described in Eq. (2);

$$H = \theta_a - \theta_r \quad (2)$$

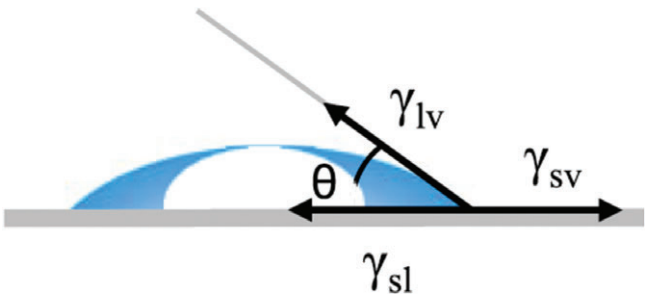

FIGURE 1 The triple-phase line; where θ is the contact angle and γ_{lv}, γ_{sv} and γ_{sl} are the liquid-vapour, solid-vapour and solid-liquid interfacial tensions, respectively. Adapted from ref. [13] with permission of Springer

There have been many studies in relation to the cause of CAH [5, 18, 19], all of which point to a similar conclusion; it arises from surface heterogeneity and roughness, therefore, when experimenting with a smooth and homogeneous solid surface, the CAH should, in theory, be negligible [20, 21]. There are other approved models relating to contact angles observed from rough and heterogeneous surfaces, such as, Wenzel [22] and Cassie and Baxter [23], however, they would not be relevant in biomedical vibrational spectroscopy, where these types of surfaces are not wholly applicable as optical components, but may be of interest when considering enhanced biofluid spectroscopy [24].

3 | COMMON PATTERNS

One of the most common patterns seen in literature is a dense, ring-like shape around the periphery of the drop. Deegan et al. [2, 25] showed that as a liquid droplet evaporates, capillary flow pushes the suspended particles outwards from the centre towards its edge. The rounded particles start to pack closely together, and once all the liquid evaporates, a circle of solid deposits is left behind. This is now widely known as the "coffee-ring effect" and is seen in the majority of colloidal solutions [26, 27]. This theory suggests that when the contact line is pinned, the liquid from the centre of the drop must move radially outwards to replenish the evaporated liquid at the edge [25]. For example, Figure 2 describes that for a droplet with fixed radius, the volume of the droplet will decrease over time, in turn decreasing the contact angle. In this dynamic, the dried solute particles ensure the radius of the drop remains constant. It was later suggested that pattern formation is dependent on the ability to self-pin and is influenced by solute or surfactant concentration, particle size and ionic strength [28]—this has been confirmed in other studies [29–31].

This theory neglects important thermal processes that influence droplet drying. The Marangoni effect is induced by a surface tension gradient, where the particles move from low to high surface tension dependent upon temperature variations along the interface [32]. This flow can reverse the coffee-ring effect, causing deposition to occur in the centre of the drop rather than the periphery [33]. Hu and Larson [34] showed that for a coffee-ring deposit to be observed, not only does the contact line have to be pinned, but the Marangoni flow must also be suppressed. In their study, they showed that Marangoni flow is dominant over capillary flow for organic systems, like octane (Figure 3), whereas in sessile water droplets, the Marangoni effect was not as prominent. Hu and Larson concluded that an inward radial flow will occur with a large contact angle (deposition in the centre), whereas the outward radial flow will dominate with a small contact angle (coffee-ring effect). They suggested

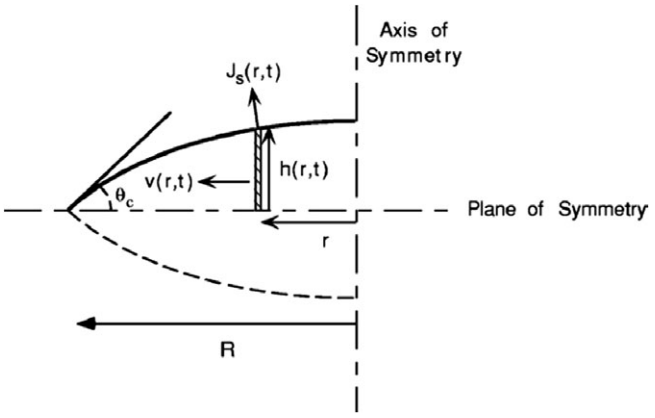

FIGURE 2 Evaporation model; where θ_c is the contact angle, v is the vertically averaged radial flow, h is the air-liquid interface, r is the radial distance and J_s represents the rate of mass loss, per unit surface area per unit time, from the drop by evaporation. Reprinted with permission of ref. [25] Copyright 2017 American Physical Society

that if the Marangoni effect could be controlled by redirecting the evaporation-driven deposition, then, in turn, the pattern formation could also be controlled. This has been confirmed where addition of surface-absorbed polymers or surfactants controls the Marangoni effect, resulting in a more uniform deposition [35].

Marangoni flow has been studied experimentally and through numerical and computational modelling [1, 36, 37]. The simulations in these studies have the advantage of viewing the flow effects in more detail [38–40]. This behaviour is common in pure liquids, but has been found to be far more complex in multiple component systems [41]. One study documented multiple phase transitions in an evaporating Ouzo drop – a tertiary mixture (water, ethanol and anise oil). The transparent drop started to decrease in size as the ethanol began to evaporate first, then oil microdroplets started to nucleate causing a transition into a milky-white coloured emulsion. An oil ring formed around the remaining water, caused by Marangoni forces, once all the ethanol had been removed. Finally, the water evaporated and a small cap shaped oil drop remained [42].

Another model was produced where the final drop pattern becomes deformed [43]. In this experiment, the drying process of a polymer solution on a substrate, which held a large contact angle for the droplet, was evaluated. Emphasis was placed on the importance of surface material, as when dropped on uncoated glass, a ring deposit was observed, whereas after coating the glass with hydrophobic material, the deformed "dot" pattern was produced. The dot pattern was essentially a large dimple in the middle of the drop, but its severity seemed to change with polymer concentration. A "piling-buckling model" was described, consisting of 3 stages; first the contact line pins, causing the contact angle to decrease with evaporation at the drop periphery—agreeing with Deegan et al. [25] model; but then the contact line moves as the contact angle recedes, and in order to keep the contact angle constant the droplet starts to shrink; and finally the contact angle becomes pinned from the polymer accumulation at the edge, leaving a deformed pattern [43].

Droplets leaving behind multiple rings have also been observed [44]. It has been proven that by adding TiO_2 nanoparticles to volatile liquid drops, for example, ethanol, "stick-slip" pinning of the triple-line occurs. The same type of pinning/depinning behaviour was observed by Parsa et al. [45], when they evaporated water droplets containing CuO nanoparticles on a silicon substrate. Multiple rings appeared when dried at extremely high temperatures (91°C), however, when evaporated at 25°C, the addition of the CuO nanoparticles suppressed the coffee-ring effect and left an evenly spread pattern. They also tested the evaporation at 47°C, 64°C and 81°C – where "dual-ring" stains were evident. The formation of the dual-ring pattern is described in Figure 4. The edge pins so naturally the nanoparticles move outwards. A number of these pack together but some move back radially to the top of the drying droplet. Over time the

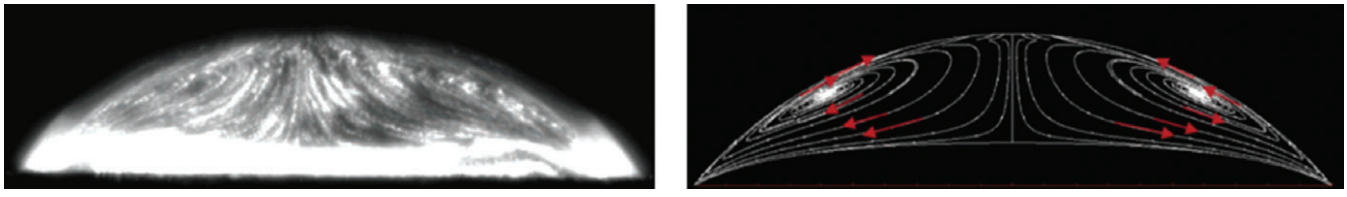

FIGURE 3 Experimental and theoretical flow field images of a drying octane droplet. Red arrows indicate the Marangoni flow. Adapted from ref [34]. Copyright 2017 American Chemical Society

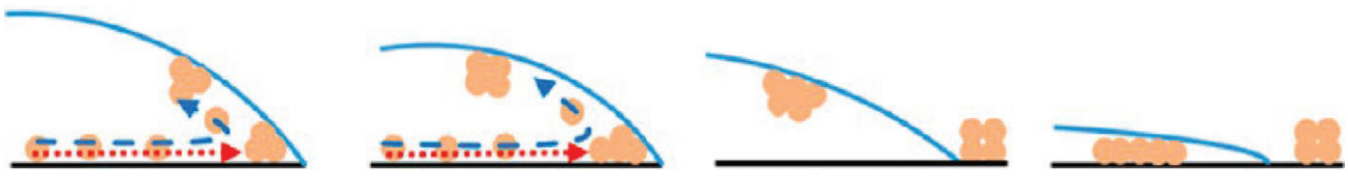

FIGURE 4 Formation of the dual ring pattern. Reprinted with permission from ref. [45] Copyright 2017 American Chemical Society

contact line becomes depinned and leaves behind a peripheral ring. This process occurs again, leaving behind the secondary ring, and hence, the "dual-ring" pattern [45].

In more complicated systems – such as salt solutions and biological fluids – phase changes occur, where the evaporating liquid will turn to either solid or gel. These types of drops generally end up cracking, leaving a wide variety of different patterns. The evaporation, gelation and cracking of drops of bovine serum albumin (BSA)—salt solution have been investigated [46], and the initial crack spacing and the gelation time have been found to be dependent on protein concentration. Yakhno [4] followed on from this study examining BSA-salt solution drops (7% weight per volume) via optical and atomic force microscopy. Six to eight drops (3 μL in volume) of each sample were pipetted onto clean glass slides and left to dry at room temperature. It was deduced that initially a solid protein ring forms round the edge of the drop, while a semi-liquid gel exists in the centre. Salt crystallisation of the gel matrix then follows shortly after. It was noted that after 2 to 3 days of drying, protein precipitates and clusters arranged at the core of the drop. Figure 5 shows the different concentric zones observed; (1) film of homogeneous protein film, (2) single protein precipitates and their clusters, (3) gel and (4) the zone of salt crystals in shrinking protein gel. In the same study, a gelatine-salt solution was examined, and this produced the same type of pattern. Salt-free solutions of BSA and gelatine were also analysed, but no protein structures were optically visible, therefore Yakhno concluded the protein structures could only be viewed in the presence of salt.

The same type of gelation and cracking behaviour is often found when drying biological fluid drops. Biofluids (blood, saliva, tears, etc.) contain hundreds of different components; such as proteins, enzymes, lipids and electrolytes, therefore the drop patterns can become even more complex [7]. On inspection of dried tear drops [47], a range of crystals were observed at the centre of the drop, with proteins and mucins appearing at the periphery. Various types of crystals have also been seen in dried drops of synovial fluid [48]. In a later study, Yakhno et al. [49] described the morphological changes of phase transitions in blood serum drops. First the dome flattened, causing the proteins to aggregate at the periphery; then the conversion zone formed which then initiated cracking; followed by the central zone formation and finally the phase transitions of salts.

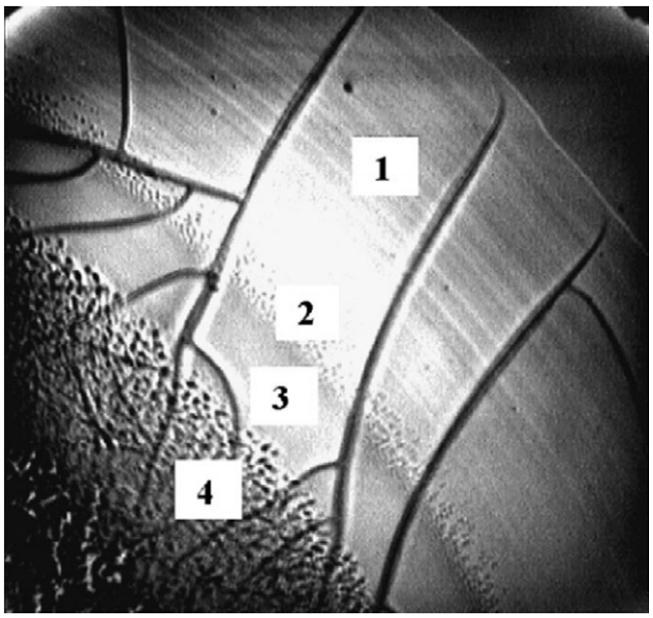

FIGURE 5 Concentric zones in dried BSA-salt solution. Replicated from ref [4] with permission of Elsevier

Another phenomenon that applies to solutions which contain many different proteins is the Vroman effect [50]. Vroman and Adams realised that when a drop is applied to a solid surface, low molecular weight (smaller) proteins attach to the surface quickly, but these proteins may be displaced by larger protein molecules through protein exchange. For example, it was shown that for a sample of blood plasma; low molecular weight albumin attached to a surface first, then a series of displacements occurred, before finally, the adsorption of high molecular weight kininogen [51]. Many proteins are also prone to changing their conformation during surface adsorption [54]—conformation changes in fibrinogen, immunoglobulinG, α-chymotrypsin and albumin have all been observed [52]. It has been shown that this type of behaviour applies during the evaporation of blood plasma [53], but it would also be relevant for most other biofluids droplets, due to the abundance of proteins that exist within.

Proteins bind to surfaces by forming various physical interactions, for example, electrostatic interactions and hydrogen bonds [54]. Efficiency of the exchange of proteins is believed to be dependent on the type of surface (hydrophobic/hydrophilic) and the conformation of the adsorbed protein at the surface [52]. Despite widespread research into competitive protein exchange, it is still not well understood and there is no existing model that can fully explain the interactions [3]. One model suggests the smaller surface attached proteins desorb naturally into solution, leaving space on the surface for adsorption of the larger proteins [55]. However, protein exchange exists even on hydrophobic surfaces, on which stronger bonds with the proteins are formed [56]. Even in studies involving hydrophilic surfaces, this model has not been found to fully explain the desorption behaviour, indicating that rapid exchange must be taking place. It has been suggested that some larger proteins must have higher surface affinity and flexibility than smaller ones making it easier to adsorb with more surface contacts, but the exact mechanism through which the exchanges occur is still unknown [57]. One interesting theory involves the larger protein binding to the initially absorbed layer of the smaller protein forming a transition complex. Once bound, the complex tilts vertically exposing the smaller protein to the solution, then it desorbs into solution [58]. This

is only one of the many theories published in recent years, therefore a better understanding of this process could aid in many applications, such as disease diagnosis [3].

4 | BIOFLUID PATTERN ANALYSIS FOR DISEASE DIAGNOSIS

There have been several studies exploring pattern formation in dried biofluids as a means of disease diagnosis. Rapis [59] was the first to suggest that the morphological patterns left by dried blood plasma drops could be useful for diagnosing disease. Martusevich et al. [60] agreed with this concept, suggesting that the pattern left behind from a blood drop is dependent on a person's health. They noted that characteristics of the blood patterns from a healthy person differed from those with a blood disease, for example, both hepatitis B and C. Differences between the blood serum patterns of healthy individuals, and those of patients with gastrointestinal and cardiovascular diseases have been observed in other studies [61, 62]. Brutin et al. [63] showed that samples from various patients – healthy, anaemic and hyperlipidemic—resulted in distinguishable patterns. The samples of whole blood—spotted on a glass surface—from the healthy patients formed larger cracks than those seen in the diseased samples. The appearance of the corona (the section between the centre and the periphery) was also dissimilar, with the anaemic samples leaving a lighter colour than the controls, whereas the samples from the patients with hyperlipidaemia left a thick and greasy layer, as shown in Figure 6.

The morphological features of dried blood serum drops from patients in various disease states, including breast and lung cancer, hepatitis and paraproteinemia, also exhibited considerable differences in the dried patterns [49]. In the same study, plasma samples from women postnatal (with in-time and premature birth), women with normal pregnancy and women with threatened premature delivery were also successfully differentiated. The potential use of blood drop pattern analysis in medical diagnostics has thus been thoroughly established by observing fundamental droplet drying dynamics. There have been studies looking into the differences in enzyme concentration (eg, lysozyme) in tear drops to diagnose eye diseases [64–66].

5 | PATTERN CONTROL

Despite ring formation being preferential in some applications, such as inkjet printing [6], it can be considered undesirable in others. For example, in DNA microarrays – drying drops of DNA can become concentrated in a narrow ring round the outside, with almost no DNA present at the core [67]. For this reason, numerous researchers have looked at how to suppress the coffee-ring effect. Temperature was shown to be a depending factor in a study carried out by Yanan Li et al. [68] They found that drying a droplet of solution—water with added monodispersed hydrophilic polystyrene nanospheres—at a higher temperature (75°C c.f. 25°C) reversed the coffee-ring effect, and caused the particles to be deposited uniformly over the whole drop. Originally, they believed this was due to the increased temperature causing a higher Marangoni effect, but as other studies have shown, Marangoni flow is relatively weak in water droplets [34]. It was deduced that the suppression of the coffee ring was likely to be due to a process described as "interface capture effect." When exposed to extreme temperatures, the particles are captured by the rapidly descending interface, forming a continuous particle layer, depositing across the whole drop surface (Figure 7).

The use of electric fields [69, 70] and electrowetting [71] have been shown to be an efficient tool to suppress the coffee-ring effect, specifically in complex fluids, for example, those containing DNA or large colloids. Changing the shape of the particles can cause differences in the final pattern [31]. By altering spherical particulates to anisotropic ellipsoids, strong particle-particle interactions between the ellipsoids form loosely packed structures on the air-water interface, preventing migration to the periphery, and hence, cause a more uniform distribution [31]. This was emphasised in a study by Li et al. [72], where complimentary target DNA was added to microspheres functionalized with single strand oligonucleotide probes, leading to DNA hybridization. This generated non-spherical agglomerates – which resist capillary flow – and resulted in a more even deposition. CAH has been utilised in order to suppress the coffee-ring effect [73]. Different types of polymers were analysed, and the type of stain left was shown to be dependent on both the surface activity of solutes, and the CAH of the substrates. For example, concentrated stains appeared for polymers that exhibit weak CAH, and conversely, the coffee-ring effect was evident in polymers with strong CAH.

A numerical model which combined fluid dynamics, heat transfer and transport mechanisms was proposed by Bhardwaj et al. [74], in an attempt to understand the deposition that occurs during the evaporation of a nanolitre colloidal solution. Simulations were performed and the results were compared experimentally using the same parameters. The evaporation times and flow fields that were calculated numerically were in good agreement with both published data and their own experiments. Numerical modelling, therefore, could potentially be a useful tool in predicting pattern formation [74]. Some researchers have also looked at the effects of varying the surface material [75, 76]. The change in evaporation behaviour of pure blood drops when dried on 3 different substrates – glass, gold and aluminium – has been examined [77]. The evaporation dynamics were expected to be the same for all 3 surfaces, as the solvent

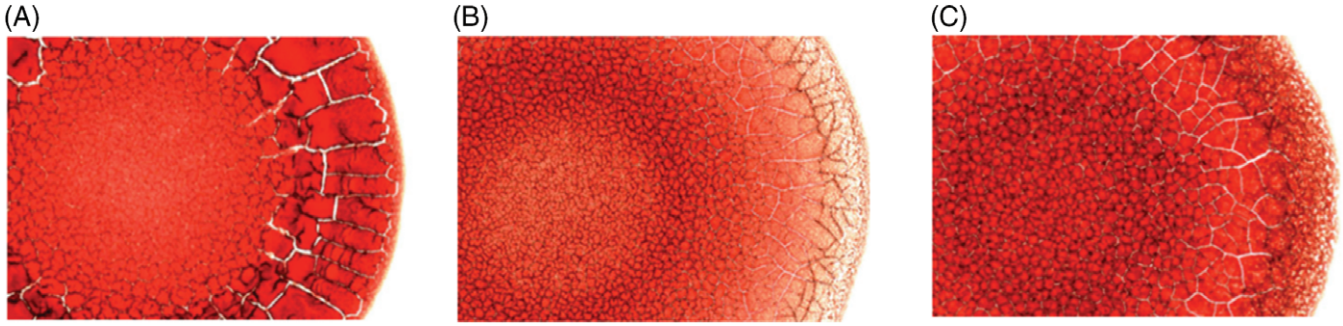

FIGURE 6 Blood drop patterns observed from (A) healthy, (B) anaemic and (C) hyperlipideamic patients, respectively. Adapted from ref. [63] with permission of Cambridge University Press

vapour's diffusion to the outside air was the limiting factor, but instead they observed significant differences due to the change in wettability. Glassy skins were formed around the droplet surfaces on the metal substrates (Au and Al), whereas on the glass substrate, the formation of a skin along the drop periphery with an inward gelation front was evident.

The effect of relative humidity (RH) on the spreading behaviour of a drying blood droplet has been investigated [78], and it was confirmed that humidity influences both the contact angle and wetting diameter, and hence the final deposition pattern. By varying the humidity during evaporation, the contact angle decreased as a function of humidity. The result of this can be visualised in Figure 8, where increasing humidity stabilised the uniformity of the sample cracks. In a further study, Bou Zeid et al. [79] examined the influence of evaporation rate on the formation of cracks in the dried blood spots. Their experiments showed that the evaporation rate has an effect on the structural distribution of plaques (specific crack patterns) and the final diameter of the plaques at the end of the evaporation. Radial cracks were observed at the high drying rate (low RH) whereas destructured cracks were evident at lower evaporation rates (high RH). They also concluded that the length of the corona remains constant through alteration of the humidity/evaporation rate. The findings from Bou Zeid's work could be beneficial for biomedical vibrational spectroscopy, as surface heterogeneity is one of the main experimental implications found in spectroscopic analysis.

6 | BIOMEDICAL VIBRATIONAL SPECTROSCOPY

Biomedical vibrational spectroscopy is an emerging field in the quest for early disease diagnosis [80–84]. Spectroscopic techniques have become of great interest to medical researchers for various reasons; analysis is rapid, cheap and non-invasive, instruments are easy to operate, but more importantly, they have the ability to characterise the presence of biomolecules and generate a biochemical fingerprint [85]. Also, it has been shown that protein imbalances in biofluids can give an indication of disease states [86]. There have been many proof-of-principle experiments highlighting the potential use of spectroscopic techniques in the clinic, mainly focused on Raman and infrared (IR) techniques [87–89].

Raman spectroscopy consists of monochromatic radiation (a laser source) interacting with a sample, which causes scattering of photons [90]. The majority of these photons are elastically scattered, known as Rayleigh scattering, resulting in no energy change. There are 2 types of inelastic Raman scattering, termed Stokes and anti-Stokes. Raman-Stokes occurs when photons transfer energy to the molecules as vibrational energy, the scattered photons exhibit energy loss, and this loss of energy corresponds to the vibrational energy levels of the molecules [91]. The incident photons can then receive energy from the vibrating molecules, increasing their frequencies—this is described as anti-Stokes scattering [81]. A Raman spectrum represents a molecular fingerprint of the sample (Figure 9), and the scattering effects are highly sensitive to any changes in cells and tissues—such as, disease states—providing a promising diagnostic and prognostic tool [89].

In IR spectroscopy, a sample is irradiated with IR light which causes atomic displacements and molecular vibrations. Various types of modalities can be used, as the IR radiation can be transmitted, reflected, internally reflected or transflected [11]. The absorption of this light excites vibrational transitions of molecules, producing IR spectra that contain a vast amount of chemical and biological information [92]. A typical IR spectrum of a biological sample (Figure 10) can quantify the levels of lipids, proteins, carbohydrates and nucleic acids present within the sample, and when coupled with data analysis, can differentiate between healthy and diseased samples [93]. The main regions of interest are usually the amide I/II peaks, and the fingerprint region (900-1900 cm^{-1}). Fourier Transform IR (FTIR) spectroscopy is thought to have the potential to be effectively translated to the clinic when combined with data analysis, due to the rapid acquisition times and high spectral quality [94, 95].

Raman spectroscopy was used by Esmonde-White et al. [48] to examine synovial fluid for osteoarthritis

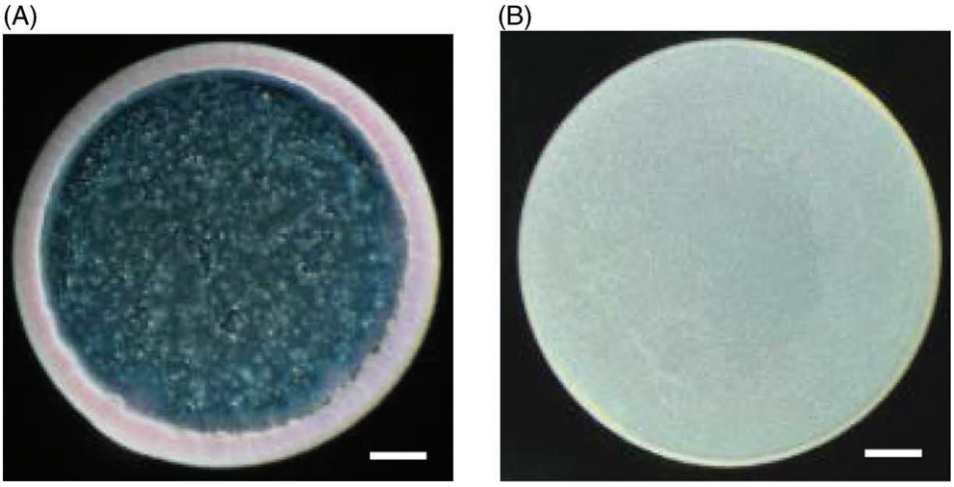

FIGURE 7 SEM images of the dried droplets at (A) 25°C and (B) 75°C. Adapted from ref. [70] with permission from Nature Publishing Group

detection. They found that specific Raman bands could describe different secondary protein structures, which in turn could detect changes in synovial fluid from the osteoarthritic patients. The protein concentrations in tear droplets have also been analysed by Raman spectroscopy, with the aim of indicating ocular disease [96]. Through the use of IR analysis, healthy serum samples have been successfully separated from those with hepatic fibrosis with a sensitivity of 92% and a specificity of 100% [97]. A recent pilot study explored the use of IR spectroscopy in the diagnosis of rheumatoid arthritis, in which the initial results seemed promising, for a disease normally so difficult to diagnose [98].

With cancer rates rising by around 3% each year in the United Kingdom [99], and increasing in a similar trend globally, the demand for a reliable early detection method has never been higher. There have been studies relating to the detection of various cancer types using Raman and IR techniques; such as lung, breast, bladder and ovarian cancers [100–103]. Taleb et al. [104] used micro-Raman spectroscopy to discriminate patients with and without hepatocellular carcinoma—the most common type of primary liver cancer. They analysed both dried serum drops and freeze-dried serum, reporting overall rates of accuracy of 84.5% to 90.2% and 86% to 91.5%, respectively. Early work on the diagnosis of melanoma skin cancer using a fibre-optic Raman probe gained 100% sensitivity and 91% specificity for discriminating tumours from normal skin [105]. Malignant tumour tissue and healthy bronchial (lung) tissue have also been found to be distinguishable using Raman spectroscopy [106]. The use of IR discriminating between different subtypes and cancer grades has also been examined. Baker et al. [107] were able to differentiate low-grade, intermediate and aggressive prostate cancer with sensitivities and specificities of 83.6% and 86%, respectively. Different sub-variants of urinary bladder carcinomas have been diagnosed via FTIR analysis, as the spectroscopic signals changed dramatically depending on the sub-variant analysed, allowing sub-classification [108]. Findings from these studies may allow better treatment planning and improve patient prognosis.

The earlier detection of cancers historically more difficult to diagnose, such as, brain cancer, has also been examined [109, 110]. Using attenuated total reflection-FTIR (ATR-FTIR) coupled with support vector machine (SVM) analysis, to distinguish between cancerous gliomas and non-cancer, Hands et al. were able to achieve sensitivities and specificities of 91.5% and 83.0%, respectively [95, 111]. The use of Raman spectroscopy in diagnosing metastatic brain cancer, and determining the primary site of origin (eg, lung, breast, colon, etc.) by analysing the cancerous brain tissue, has been investigated. Interesting differences in the spectra of metastatic and primary brain cancer samples were also observed [112].

The volume of papers published in the field emphasises the promise of vibrational spectroscopy in medical

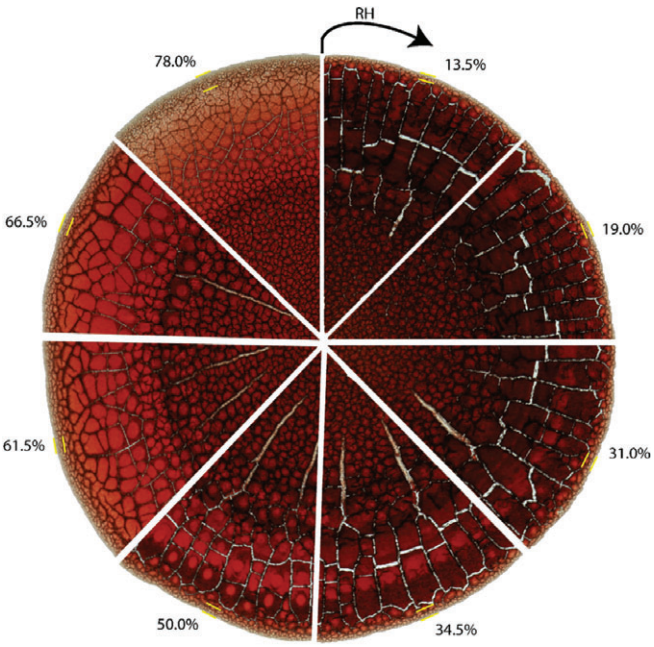

FIGURE 8 Change in deposition with the increase of relative humidity. Replicated from ref. [78] with permission of Elsevier

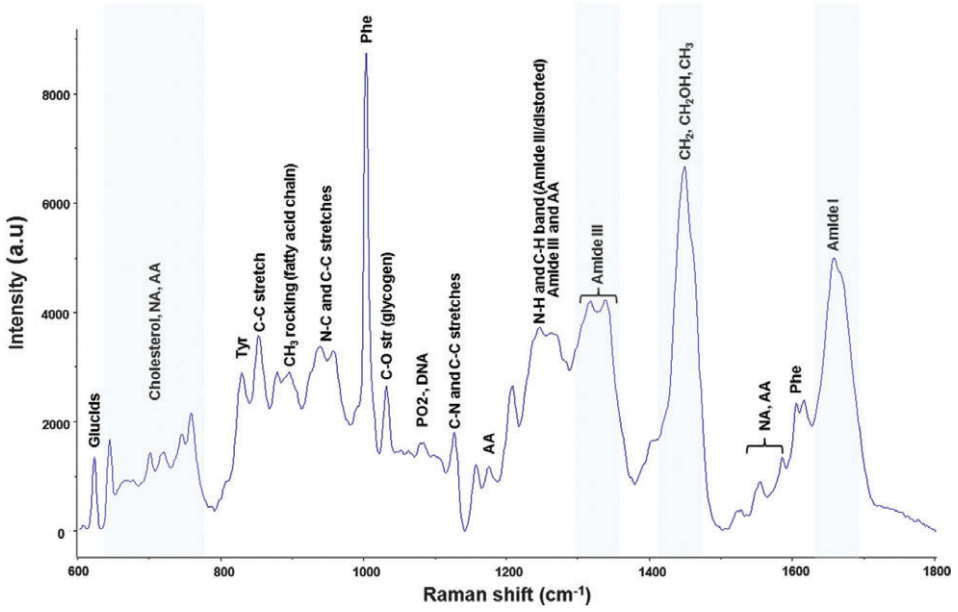

FIGURE 9 Raman spectrum derived from a dried blood serum drop with spectral assignments. Replicated from ref. [11] with permission of Royal Society of Chemistry

diagnostics. However, the complex patterns formed from dried biofluid drops have proven to be problematic in these types of studies, and the poor understanding of the fundamentals of drop drying is barring efficient translation to the clinic. The chemical heterogeneity across the drop surface, the presence of cracks and variance in sample thickness has been found to cause distortions to both Raman and IR spectra. Hughes et al. [12] used transmission mode IR to analyse 25 different points on a single dried blood serum sample at various random locations; there were differences in absorption values observed in the amide I and II regions (emphasised in Figure 11A) indicating that the protein structure differed across the droplet (Figure 11B). This lead to the suggestion that for the technique to be utilised fully, the proteins and other macromolecules must be spread uniformly across the sample. As a result of the inhomogeneous deposition during the drying process, variance in sample thickness across singular blood serum drops has also been shown to cause shifting of peaks. Bonnier et al. [113] observed a coffee-ring pattern, after a 20 µL spot of diluted blood serum (1 in 15 dilution) was air dried on a calcium fluoride substrate. This allowed 3 different IR measurements to be taken; from the inner, middle and outer parts of the ring, resulting in shifts in peak positions in the 1500 to 1000 cm^{-1} region. The band intensity ratios also differed across the ring due to the inconsistent spread of protein molecules (Figure 12).

Likewise, similar effects have been encountered when collecting Raman spectra from dried drops. Esmonde-White et al. [114] noticed spectral differences due to drop thickness, in the analysis of hyaluronic acid (HA)—a major component in synovial fluid. Various concentrations of aqueous HA drops were analysed using surface-enhanced Raman spectroscopy (SERS). The band corresponding to the symmetric C—O—C linkage stretch (945 cm^{-1}) was found to increase at the higher concentrations, indicating a rise in concentration will affect not only the drop appearance, but also the resulting spectra. In a later study, the inhomogeneous deposition of proteins in dried synovial fluid drops produced spectral alterations – depending on the location that was analysed [48]. For both Raman and IR, it can also be assumed that when irradiating a cracked sample, there would be some undesirable scattering of light, which is comparable with the baseline variations observed from a sample edge during tissue analysis [115].

Compared to other IR techniques, the ATR-FTIR approach is preferable for the analysis of water containing samples, as a consequence of the smaller pathlength into the sample, defined by the penetration depth of the evanescent wave, which in turn reduces the spectral contributions of water [93]. Despite the advantages of such an approach,

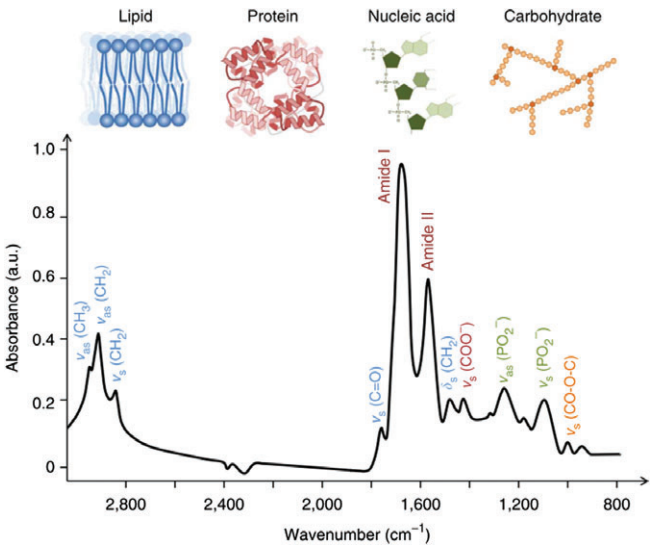

FIGURE 10 Biological spectrum showing biomolecular peak assignments. Replicated from ref. [93] with permission from Macmillan Publishers Ltd

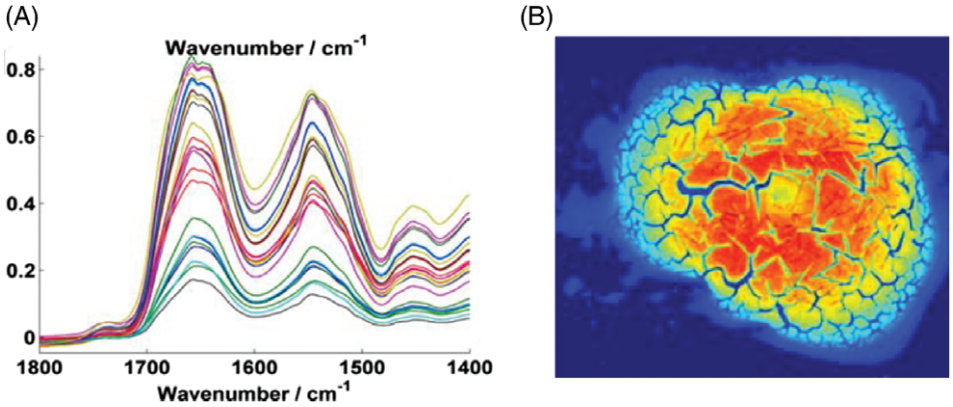

FIGURE 11 The differences observed in (A) the Amide I and II peaks and (B) the protein absorbance. Adapted from ref. [12] with permission of Wiley

when analysing liquid samples, or those that have not fully dried, water associated peaks are still apparent in the fingerprint region. This can be an issue when analysing body fluids, as the water features can obscure the protein absorbance peaks, potentially leading to false interpretation of the spectra [86]. It would also be expected that the measurements taken would not be fully representative of the whole drop, in other words, components that exist in low concentration may not be detected at the surface until fully dry. Again, this could be related to the Vroman effect [116], where the higher molecular weight proteins do not attach to the surface until sometime after the drop has been spotted. Hydration effects have been emphasised in another study, where 2 additional states of urea were evident in the IR spectra of partially dried urine samples [117]. It is, therefore, more common to use dried sample drops when analysing bodily fluids through IR spectroscopy, as the absorbance of proteins dominates that of the water features—namely in the Amide I and II regions (Figure 13) [86]. Conversely, Raman spectroscopy is more suitable for wet samples, as water is a weak Raman scatterer and causes little interference in areas of biological interest [91]. Although, this can be dependent on the type of biofluid being analysed—for example, a wet sample of whole blood will produce a different spectral signature to that of a dried sample. This is thought to be due to the coagulation process that occurs as blood dries, varying the haemoglobin and fibrin levels [118].

There have been studies suggesting ways around these experimental limitations. Prior to investigating clinical variations between serum samples, the effect of serum dilution on the deposition patterns has been examined using FTIR imaging and high-throughput FTIR [119]. The spectral images visibly showed the increased homogeneity for the diluted samples, with both the coffee-ring and cracking patterns not as prominent as more concentrated samples (Figure 14). In this particular example, a dilution of 1 in 3 was deemed to provide the best results as sample homogeneity was optimised, but not at the expense of spectral quality. To ensure complete dryness, samples were left at room temperature for 1 hour, and thus do not represent the drying conditions feasible for a high-throughput process [120].

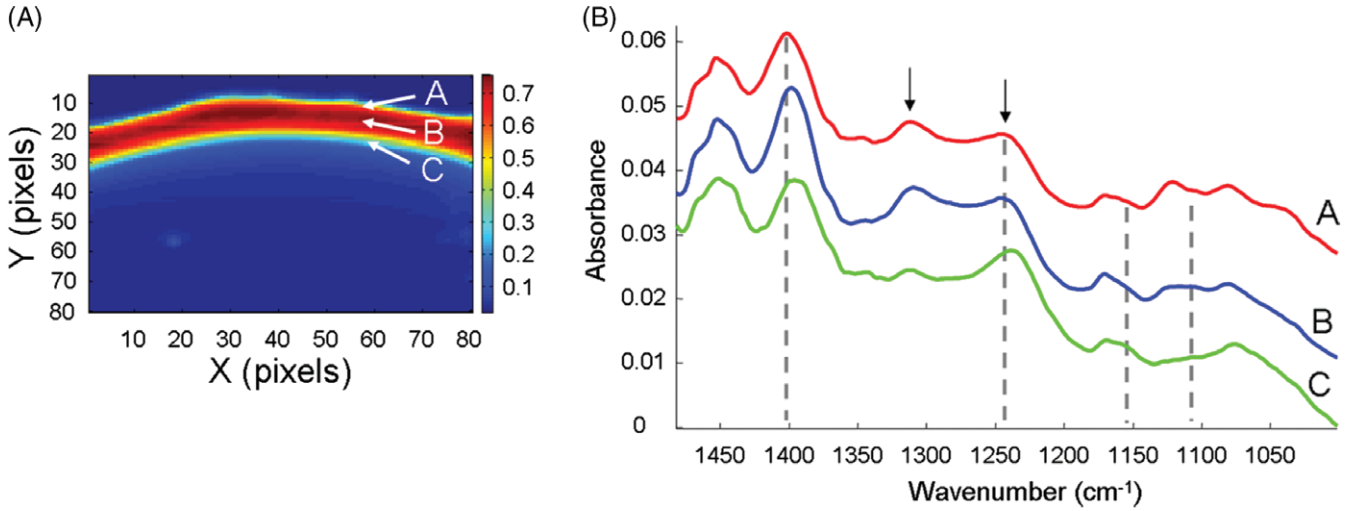

FIGURE 12 Infrared image collected for a 20 μL drop of 1 of 15 diluted human serum after air drying. Spectra, zoomed to 1500 to 1000 cm^{-1}, collected in each region; A, B and C. Dotted line shows peak shift and arrows show change in band intensity ratios. Duplicated from ref. [113] with permission of Wiley

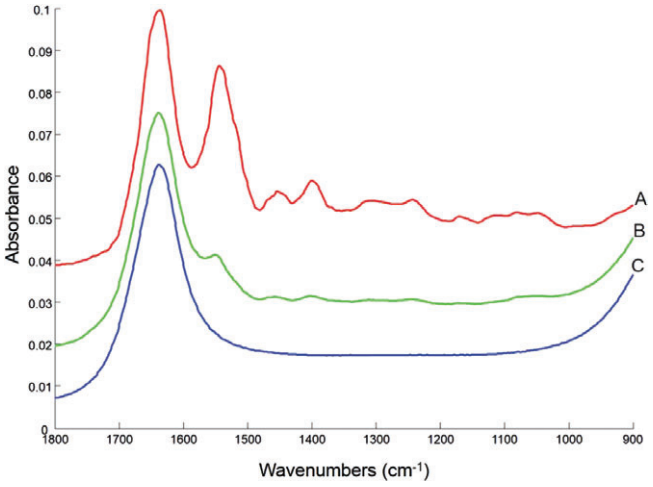

FIGURE 13 IR spectra of; (A) whole blood serum after 10 minutes of drying, (B) whole blood serum before drying, and (C) of Milli-Q water where the baselines have been offset for comparison. Replicated from ref. [86] with permission of the Royal Society of Chemistry

Various considerations must be made in order to gain reliable reproducibility. The type of substrate and biofluids being analysed, how the sample is collected and deposited, the drying conditions, the volume and dilution factor are just some of the aspects that need to be considered to combat intra- and inter-centre variabilities. It has been confirmed that reducing the sample volume can improve drying time—at room temperature (~18°C) it takes approximately 8 minutes for 1 μL of whole serum to fully dry [109]. Although, from a clinical perspective this is still a rather long waiting time, and so the use of a humidity chamber to accelerate drying time could prove to be far more efficient [78].

Bonnier et al. [113, 121] had an interesting view on the issues involved with both sample drying and the acquisition of spectra from wet samples. Instead of trying to eradicate these pre-analytical problems, they suggested the use of alternative approaches to record quality data, without the requirement of water-free samples. They altered the sample concentration by centrifugal filtration, which seemed to improve the spectral quality. The higher molecular weight proteins, such as human serum albumin (HSA), are filtered out resulting in enrichment of the lower molecular weight proteins that are of greater diagnostic value [122]. The concept of automated sampling has been utilised by Ollesch et al. [123], where the homogeneity of spotted samples was found to be far greater. They used a robotic dispensing system which provided highly reproducible spectra, managing to avoid the uneven coffee-ring effect. Preprocessing and multivariate analysis techniques have also been employed to dismiss spectral differences [95, 124].

7 | CONCLUSION

Liquid drop drying is a highly complex process which to this day is not completely understood. Despite the several models that have been established, it is unknown exactly what happens to all macromolecules within the drop when the liquid evaporates. The formation of diagnostically relevant patterns has shown that a biofluid droplet itself holds a wealth of diagnostic information, with specific patterns being linked to different disease states. The spectroscopic analysis of biofluids has emerged as a powerful technique in the field of disease monitoring, but in contrast is negatively affected by droplet

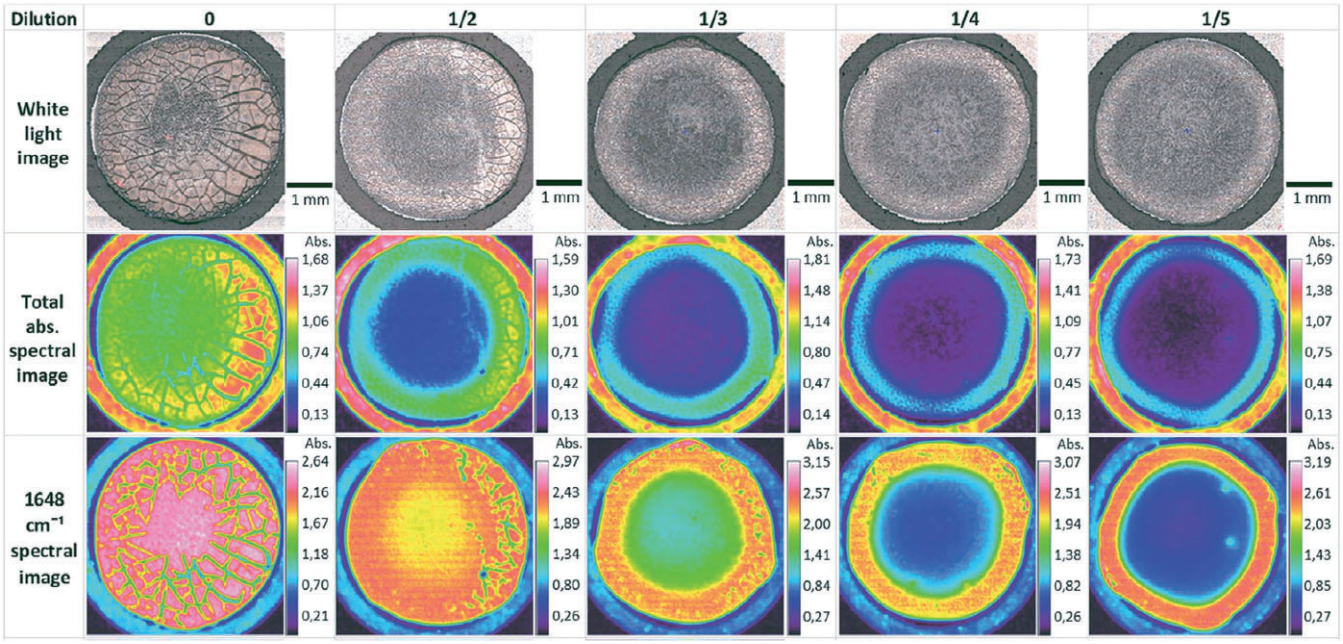

FIGURE 14 FTIR images of blood serum dilution series. Adapted from ref. [119] with permission of the Royal Society of Chemistry

inconsistencies largely associated with heterogeneous drying. Biochemical variance across a liquid drop can be detected using spectroscopic techniques such as transmission or ATR-FTIR, and cracked surfaces across a drop can generate spectral distortions often in the form of baseline discrepancies. With regards to the research outlined in this review, it could be concluded that the potentially "optimal" conditions for depositing a biofluid drop—for example, blood serum – for use in clinical spectroscopy would be a small, diluted aliquot of serum (1 μL) spotted on a smooth, flat and homogeneous surface, at an elevated temperature or high humidity in order to result in a more uniformly spread sample, with a faster drying time. Optimisation of this process in conjunction with full comprehension of the fluid dynamics of drying is important for advancing the field of biomedical spectroscopy. A model that could provide a clear picture of how and when the molecules interact with the surface would aid our understanding of the concept, and allow a more efficient and effective transition into the clinic.

ACKNOWLEDGMENTS

The authors would like to thank the EPSRC (EP/L505080/1) for funding.

AUTHOR BIOGRAPHIES

Please see Supporting Information online.

REFERENCES

[1] R. Savino, D. Paterna, N. Favaloro, *J. Thermophys. Heat Transfer* **2002**, *16*, 562.
[2] R. D. Deegan, O. Bakajin, T. F. Dupont, G. Huber, S. R. Nagel, T. A. Witten, *Nature* **1997**, *389*, 827.
[3] S. L. Hirsh, D. R. McKenzie, N. J. Nosworthy, J. A. Denman, O. U. Sezerman, M. M. M. Bilek, *Colloids Surf. B Biointerfaces* **2013**, *103*, 395.
[4] T. Yakhno, *J. Colloid Interface Sci.* **2008**, *318*, 225.
[5] J. Krumpfer, T. J. McCarthy, *Faraday Discuss.* **2010**, *146*, 13.
[6] Y. Choi, J. Han, C. Kim, *Korean J. Chem. Eng.* **2011**, *28*, 2130.
[7] R. Chen, L. Zhang, D. Zang, W. Shen, *Adv. Colloid Interf. Sci.* **2016**, *231*, 1.
[8] J. Sobek, C. Aquino, W. Weigel, R. Schlapbach, *BMC Biophys.* **2013**, *6*, 8.
[9] P. Takhistov, H.-C. Chang, *Ind. Eng. Chem. Res.* **2002**, *41*, 6256.
[10] R. Anthony Shaw, Sarah Low-Ying, Angela Man, et al. Infrared Spectroscopy of Biofluids in Clinical Chemistry and Medical Diagnostics. in *Biomedical Vibrational Spectroscopy*, John Wiley Sons Inc, Hoboken, NJ **2008**, p. 79.
[11] M. J. Baker, S. R. Hussain, L. Lovergne, V. Untereiner, C. Hughes, R. A. Lukaszewski, G. Thiéfin, G. D. Sockalingum, *Chem. Soc. Rev.* **2016**, *45*, 1803.
[12] C. Hughes, M. Brown, G. Clemens, A. Henderson, G. Monjardez, N. W. Clarke, P. Gardner, *J. Biophotonics* **2014**, *7*, 180.
[13] Y. Yuan, T. R. Lee, Contact Angle and Wetting Properties. in *Surface Science Techniques*, Vol. *51*, Springer, Berlin, Heidelberg **2013**.
[14] T. Young, *Philos. Trans. R. Soc. Lond.* **1805**, *96*, 65.
[15] W. Abdullah, J. S. Buckley, A. Carnegie, et al. *Oilfield Rev.* **2007**, *19*, 44.
[16] S. M. Burkinshaw, *Theoretical Aspects of Textile Coloration*, John Wiley & Sons Inc: Hoboken, **2016**.
[17] Crawford, R. J. & Ivanova, E. P. *Superhydrophobic Surfaces*, Elsevier: Amsterdam, Netherlands, **2015**.
[18] R. E. Johnson Jr. , R. H. Dettre, *J. Phys. Chem.* **1964**, *68*, 1744.
[19] L. Gao, T. J. McCarthy, *Langmuir* **2006**, *22*, 6234.
[20] C. Atae-Allah, M. Cabrerizo-Vílchez, J. F. Gómez-Lopera, J. A. Holgado-Terriza, R. Román-Roldán, P. L. Luque-Escamilla, *Meas. Sci. Technol.* **2001**, *12*, 288.
[21] A. W. Neumann, *Adv. Colloid Interf. Sci.* **1974**, *4*, 105.
[22] R. N. Wenzel, *Ind. Eng. Chem.* **1936**, *28*, 988.
[23] A. B. D. Cassie, S. Baxter, *Trans. Faraday Soc.* **1944**, *40*, 546.
[24] Z. A. Nima, A. Biswas, I. S. Bayer, F. D. Hardcastle, D. Perry, A. Ghosh, E. Dervishi, A. S. Biris, *Drug Metab. Rev.* **2014**, *46*, 155.
[25] R. D. Deegan, O. Bakajin, T. F. Dupont, G. Huber, S. R. Nagel, T. A. Witten, *Phys. Rev. E* **2000**, *62*, 756.
[26] T.-S. Wong, T.-H. Chen, X. Shen, C.-M. Ho, *Anal. Chem.* **2011**, *83*, 1871.
[27] X. Shen, C.-M. Ho, T.-S. Wong, *J. Phys. Chem. B* **2010**, *114*, 5269.
[28] R. D. Deegan, Phys. Rev. E 2000, 61, 475.
[29] Y. Y. Tarasevich, I. V. Vodolazskaya, O. P. Isakova, *Colloid Polym. Sci.* **2011**, *289*, 1015.
[30] D. Kaya, V. A. Belyi, M. Muthukumar, *J. Chem. Phys.* **2010**, *133*, 114905.
[31] P. J. Yunker, T. Still, M. A. Lohr, A. G. Yodh, *Nature* **2011**, *476*, 308.
[32] X. Xu, J. Luo, *Appl. Phys. Lett.* **2007**, *91*, 124102.
[33] M. Schmitt, H. Stark, *Phys. Fluids* **2016**, *28*, 012106.
[34] H. Hu, R. G. Larson, *J. Phys. Chem. B* **2006**, *110*, 7090.
[35] H. Kim, F. Boulogne, E. Um, I. Jacobi, E. Button, H. A. Stone, *Phys. Rev. Lett.* **2016**, *116*, 124501.
[36] Z. Wang, P. Lu, Y. Wang, C. Yang, Z.-S. Mao, *AICHE J.* **2013**, *59*, 4424.
[37] H. Hu, R. G. Larson, *J. Phys. Chem. B* **2002**, *106*, 1334.
[38] H. Niazmand, B. D. Shaw, H. A. Dwyer, I. Aharon, *Combust. Sci. Technol.* **1994**, *103*, 219.
[39] M. Majumder, C. S. Rendall, J. A. Eukel, J. Y. L. Wang, N. Behabtu, C. L. Pint, T. Y. Liu, A. W. Orbaek, F. Mirri, J. Nam, A. R. Barron, R. H. Hauge, H. K. Schmidt, M. Pasquali, *J. Phys. Chem. B* **2012**, *116*, 6536.
[40] J. Wang, Z. Wang, P. Lu, C. Yang, Z.-S. Mao, *AICHE J.* **2011**, *57*, 2670.
[41] C. Diddens, H. Tan, P. Lv, M. Versluis, J. G. M. Kuerten, X. Zhang, D. Lohse, *J. Fluid Mech.* **2017**, *823*, 470.
[42] H. Tan, C. Diddens, P. Lv, J. G. M. Kuerten, X. Zhang, D. Lohse, *Proc. Natl. Acad. Sci. USA* **2016**, *113*, 8642.
[43] T. Kajiya, E. Nishitani, T. Yamaue, M. Doi, *Phys. Rev. E* **2006**, *73*, 011601.
[44] J. R. Moffat, K. Sefiane, M. E. R. Shanahan, *J. Phys. Chem. B* **2009**, *113*, 8860.
[45] M. Parsa, S. Harmand, K. Sefiane, M. Bigerelle, R. Deltombe, *Langmuir* **2015**, *31*, 3354.
[46] C. C. Annarelli, J. Fornazero, J. Bert, J. Colombani, *Eur. Phys. J. E* **2001**, *5*, 599.
[47] E. Pearce, A. Thomlinson, *Ophthalmic Physiol. Opt.* **2000**, *20*, 306.
[48] K. A. Esmonde-White, G. S. Mandair, F. Raaii, J. A. Jacobson, B. S. Miller, A. G. Urquhart, B. J. Roessler, M. D. Morris, *J. Biomed. Opt.* **2009**, *14*, 034013.
[49] T. Yakhno, V. Yakhno, A. Sanin, O. Sanina, A. Pelyushenko, *IEEE Eng. Med. Biol. Mag.* **2005**, *24*, 96.
[50] L. Vroman, Proteins in Blood Plasma at Interfaces. in *Interfacial Phenomena in Biological Systems*, Vol. *39*, Marcel Dekker Inc: New York, **1992**.
[51] L. Vroman, A. L. Adams, G. C. Fischer, P. C. Munoz, *Blood* **1980**, *55*, 156.
[52] M. Malmsten, *J. Colloid Interface Sci.* **1998**, *207*, 186.
[53] S. M. Slack, T. A. Horbett, *J. Colloid Interface Sci.* **1988**, *124*, 535.
[54] V. Ball, J.-C. Voegel, P. Schaaf, Mechanism of Interfacial Exchange Phenomena for Proteins Adsorbed at Solid – Liquid Interfaces. in *Biopolymers at Interfaces*, 2nd ed. (Ed: M. Malmsten), CRC Press: Boca Raton, Florida, **2003**, p. 20033926.
[55] P. Huetz, V. Ball, J.-C. Voegel, P. Schaaf, *Langmuir* **1995**, *11*, 3145.
[56] S. M. Slack, T. A. Horbett, *J. Colloid Interface Sci.* **1989**, *133*, 148.
[57] J. Wald, C. Müller, M. Wahl, W. Hoth-Hannig, M. Hannig, M. Kopnarski, C. Ziegler, *Phys. Status Solidi A* **2010**, *207*, 831.
[58] L. Heinrich, E. K. Mann, J. C. Voegel, G. J. M. Koper, P. Schaaf, *Langmuir* **1996**, *12*, 4857.

[59] E. Rapis, *Tech. Phys.* **2002**, *47*, 510.
[60] A. K. Martusevich, Y. Zimin, A. Bochkareva, *Hepat. Mon.* **2007**, *7*, 207.
[61] V. V. Shabalin, S. N. Shatokhina, *Bull. Exp. Biol. Med.* **2016**, *161*, 841.
[62] M. E. Buzoverya, Y. P. Shcherbak, I. V. Shishpor, Y. P. Potekhina, *Tech. Phys.* **2012**, *57*, 1019.
[63] D. Brutin, B. Sobac, B. Loquet, J. Sampol, *J. Fluid Mech.* **2011**, *667*, 85.
[64] Z. Xiong, *Pattern Formation in Drying Drops of Colloidal Solutions*, University of Pittsburgh: Pittsburgh, Pennsylvania, **2013**.
[65] S. Daly, T. Przybycien, R. Tilton, *Langmuir* **2005**, *21*, 1328.
[66] R. Sariri, H. Ghafoori, *Biochemistry (Mosc)* **2008**, *73*, 381.
[67] I. I. Smalyukh, O. V. Zribi, J. C. Butler, O. D. Lavrentovich, G. C. L. Wong, *Phys. Rev. Lett.* **2006**, *96*, 177801.
[68] Y. Li, Q. Yang, M. Li, Y. Song, *Sci. Rep.* **2016**, *6*, 24628.
[69] A. W. Wray, D. T. Papageorgiou, R. V. Craster, K. Sefiane, O. K. Matar, *Procedia IUTAM* **2015**, *15*, 172.
[70] A. W. Wray, D. T. Papageorgiou, R. V. Craster, K. Sefiane, O. K. Matar, *Langmuir* **2014**, *30*, 5849.
[71] H. B. Eral, D. M. Augustine, M. H. G. Duits, F. Mugele, *Soft Matter* **2011**, *7*, 4954.
[72] Y. Li, Z. Zhao, M. L. Lam, W. Liu, P. P. Yeung, C. C. Chieng, T. H. Chen, *Sensors Actuators B Chem.* **2015**, *206*, 56.
[73] Y.-F. Li, Y.-J. Sheng, H.-K. Tsao, *Langmuir* **2013**, *29*, 7802.
[74] R. Bhardwaj, X. Fung, D. Attinger, *New J. Phys.* **2009**, *11*, 075020.
[75] A. Dimitrov, C. Dushkin, H. Yoshimura, N. Kunaiki, *Langmuir* **1994**, *10*, 432.
[76] A. Chandramohan, S. Dash, J. A. Weibel, X. Chen, S. V. Garimella, *Langmuir* **2016**, *32*, 4729.
[77] D. Brutin, B. Sobac, C. Nicloux, *J. Heat Transf.* **2012**, *134*, 061101.
[78] W. Bou Zeid, D. Brutin, *Colloids Surf. A Physicochem. Eng. Asp.* **2013**, *430*, 1.
[79] W. Bou Zeid, J. Vicente, D. Brutin, *Colloids Surf. A Physicochem. Eng. Asp.* **2013**, *432*, 139.
[80] M. J. Baker, *J. Biophotonics* **2014**, *7*, 151.
[81] M. J. Baker, C. S. Hughes, K. A. Hollywood, *Biophotonics: Vibrational Spectroscopic Diagnostics*, IOP Publishing, Morgan & Claypool: San Rafael, **2016**. https://doi.org/10.1088/978-1-6817-4071-3.
[82] G. Clemens, J. R. Hands, K. M. Dorling, M. J. Baker, *Analyst* **2014**, *139*, 4411.
[83] H. J. Byrne, K. Ostrowska, H. Nawaz, et al., Vibrational Spectroscopy: Disease Diagnostics and Beyond. in *Optical Spectroscopy and Computational Methods in Biology and Medicine*, Springer, Dordrecht, **2013**.
[84] C. Hughes, G. Clemens, B. Bird, T. Dawson, K. M. Ashton, M. D. Jenkinson, A. Brodbelt, M. Weida, E. Fotheringham, M. Barre, J. Rowlette, M. J. Baker, *Sci. Rep.* **2016**, *6*, 20173.
[85] O. J. Old, L. M. Fullwood, R. Scott, G. R. Lloyd, L. M. Almond, N. A. Shepherd, N. Stone, H. Barr, C. Kendall, *Anal. Methods* **2014**, *6*, 3901.
[86] F. Bonnier, M. J. Baker, H. J. Byrne, *Anal. Methods* **2014**, *6*, 5155.
[87] K. Spalding, R. Board, T. Dawson, M. D. Jenkinson, M. J. Baker, *Brain Behav.* **2016**, *6*, e00502.
[88] K. Dorling, M. J. Baker, *Trends Biotechnol.* **2013**, *31*, 325.
[89] K. Kong, C. Kendall, N. Stone, I. Notingher, *Adv. Drug Deliv. Rev.* **2015**, *89*, 121.
[90] C. V. Raman, K. S. Krishnan, *Nature* **1928**, *121*, 501.
[91] H. J. Butler, L. Ashton, B. Bird, G. Cinque, K. Curtis, J. Dorney, K. Esmonde-White, N. J. Fullwood, B. Gardner, P. L. Martin-Hirsch, M. J. Walsh, M. R. McAinsh, N. Stone, F. L. Martin, *Nat. Protoc.* **2016**, *11*, 664.
[92] A. Barth, *Biochim. Biophys. Acta* **2007**, *1767*, 1073.
[93] M. J. Baker, J. Trevisan, P. Bassan, R. Bhargava, H. J. Butler, K. M. Dorling, P. R. Fielden, S. W. Fogarty, N. J. Fullwood, K. A. Heys, C. Hughes, P. Lasch, P. L. Martin-Hirsch, B. Obinaju, G. D. Sockalingum, J. Sulé-Suso, R. J. Strong, M. J. Walsh, B. R. Wood, P. Gardner, F. L. Martin, *Nat. Protoc.* **2014**, *9*, 1771.
[94] G. Bellisola, C. Sorio, *Am. J. Cancer Res.* **2012**, *2*, 1.
[95] B. R. Smith, K. M. Ashton, A. Brodbelt, T. Dawson, M. D. Jenkinson, N. T. Hunt, D. S. Palmer, M. J. Baker, *Analyst* **2016**, *141*, 3668.
[96] J. Filik, N. Stone, *Anal. Chim. Acta* **2008**, *616*, 177.
[97] E. Scaglia, G. D. Sockalingum, J. Schmitt, C. Gobinet, N. Schneider, M. Manfait, G. Thiéfin, *Anal. Bioanal. Chem.* **2011**, *401*, 2919.
[98] L. Lechowicz, M. Chrapek, J. Gaweda, M. Urbaniak, I. Konieczna, *Mol. Biol. Rep.* **2016**, *43*, 1321.
[99] Macmillan, *Cancer Statistics*. Macmillan Cancer Support Online, **2017**, http://www.macmillan.org.uk/_images/cancer-statistics-factsheet_tcm9-260514.pdf. [accessed 22 September 2017]
[100] M. J. Walsh, S. E. Holton, A. Kajdacsy-Balla, R. Bhargava, *Vib. Spectrosc.* **2012**, *60*, 23.
[101] B. Bird, M. Miljković, S. Remiszewski, A. Akalin, M. Kon, M. Diem, *Lab. Investig.* **2012**, *92*, 1358.
[102] K. Gajjar, J. Trevisan, G. Owens, P. J. Keating, N. J. Wood, H. F. Stringfellow, P. L. Martin-Hirsch, F. L. Martin, *Analyst* **2013**, *138*, 3917.
[103] J. Backhaus, R. Mueller, N. Formanski, N. Szlama, H. G. Meerpohl, M. Eidt, P. Bugert, *Vib. Spectrosc.* **2010**, *52*, 173.
[104] I. Taleb, G. Thiéfin, C. Gobinet, V. Untereiner, B. Bernard-Chabert, A. Heurgué, C. Truntzer, P. Hillon, M. Manfait, P. Ducoroy, G. D. Sockalingum, *Analyst* **2013**, *138*, 4006.
[105] C. A. Lieber, S. K. Majumder, D. L. Ellis, D. D. Billheimer, A. Mahadevan-Jansen, *Lasers Surg. Med.* **2008**, *40*, 461.
[106] Z. Huang, A. McWilliams, H. Lui, D. I. McLean, S. Lam, H. Zeng, *Int. J. Cancer* **2003**, *107*, 1047.
[107] M. J. Baker, E. Gazi, M. D. Brown, J. H. Shanks, N. W. Clarke, P. Gardner, *J. Biophotonics* **2009**, *2*, 104.
[108] C. Hughes, J. Iqbal-Wahid, M. Brown, J. H. Shanks, A. Eustace, H. Denley, P. J. Hoskin, C. West, N. W. Clarke, P. Gardner, *J. Biophotonics* **2013**, *6*, 73.
[109] J. R. Hands, K. M. Dorling, P. Abel, K. M. Ashton, A. Brodbelt, C. Davis, T. Dawson, M. D. Jenkinson, R. W. Lea, C. Walker, M. J. Baker, *J. Biophotonics* **2014**, *7*, 189.
[110] M. Kirsch, G. Schackert, R. Salzer, C. Krafft, *Anal. Bioanal. Chem.* **2010**, *398*, 1707.
[111] J. R. Hands, G. Clemens, R. Stables, K. Ashton, A. Brodbelt, C. Davis, T. P. Dawson, M. D. Jenkinson, R. W. Lea, C. Walker, M. J. Baker, *J. -Neuro-Oncol.* **2016**, *127*, 463.
[112] L. M. Fullwood, G. Clemens, D. Griffiths, K. Ashton, T. P. Dawson, R. W. Lea, C. Davis, F. Bonnier, H. J. Byrne, M. J. Baker, *Anal. Methods* **2014**, *6*, 3948.
[113] F. Bonnier, F. Petitjean, M. J. Baker, H. J. Byrne, *J. Biophotonics* **2014**, *7*, 167.
[114] K. A. Esmonde-White, S. V. Le Clair, B. J. Roessler, M. D. Morris, *Appl. Spectrosc.* **2008**, *62*, 503.
[115] P. Bassan, *Light Scattering during Infrared Spectroscopic Measurements of Biomedical Samples*, University of Manchester, Manchester, **2011**.
[116] L. Vroman, A. L. Adams, *J. Biomed. Mater. Res. A* **1969**, *3*, 43.
[117] K. Oliver, *Infrared Spectroscopy as a Clinical Diagnostic Method for Detection of Disease States: Developments and Applications in Kidney Diseases and Cancer Diagnoses*, University College London, London, **2015**.
[118] V. Sikirzhytski, K. Virkler, I. K. Lednev, *Sensors* **2010**, *10*, 2869.
[119] L. Lovergne, G. Clemens, V. Untereiner, R. A. Lukaszweski, G. D. Sockalingum, M. J. Baker, *Anal. Methods* **2015**, *7*, 7140.
[120] L. Lovergne, P. Bouzy, V. Untereiner, R. Garnotel, M. J. Baker, G. Thiéfin, G. D. Sockalingum, *Faraday Discuss.* **2016**, *187*, 521.
[121] F. Bonnier, H. Blasco, C. Wasselet, G. Brachet, R. Respaud, L. F. C. S. Carvalho, D. Bertrand, M. J. Baker, H. J. Byrne, I. Chourpa, *Analyst* **2017**, *142*, 1285.
[122] R. S. Tirumalai, K. C. Chan, D. R. A. Prieto, H. J. Issaq, T. P. Conrads, T. D. Veenstra, *Mol. Cell. Proteomics* **2003**, *2*, 1096.
[123] J. Ollesch, S. L. Drees, H. M. Heise, T. Behrens, T. Brüning, K. Gerwert, *Analyst* **2013**, *138*, 4092.
[124] J. Ollesch, M. Heinze, H. M. Heise, T. Behrens, T. Brüning, K. Gerwert, *J. Biophotonics* **2014**, *7*, 210.

How to cite this article: Cameron JM, Butler HJ, Palmer DS, Baker MJ. Biofluid spectroscopic disease diagnostics: A review on the processes and spectral impact of drying. *J. Biophotonics*. 2018;11: e201700299. https://doi.org/10.1002/jbio.201700299